PERGAMON

International Journal of Solids and Structures 39 (2002) 3845–3856

INTERNATIONAL JOURNAL OF SOLIDS and STRUCTURES

www.elsevier.com/locate/ijsolstr

Stability of pressure-dependent, thermally-induced displacive transformations in bi-atomic crystals

Ryan S. Elliott, John A. Shaw *, Nicolas Triantafyllidis

Department of Aerospace Engineering, College of Engineering, University of Michigan, Francois-Xavier Bagnoud Building 1320, Beal Avenue, Ann Arbor, Michigan, MI 48109-2140, USA

Received 13 February 2002

Abstract

An important property of some metallic alloys, such as NiTi, for technological applications is their coupled thermo-mechanical shape memory behavior. This is due to temperature-dependent first-order displacive (martensitic) transformations in which their crystal structures transform between a higher symmetry cubic phase and lower symmetry phases (rhombohedral, tetragonal, orthorhombic, or monoclinic).

In a recent paper, Elliott et al. (J. Mech. Phys. Solids, in press) proposed a nano-mechanical model based on temperature-dependent atomic potentials to explicitly construct an energy density $W(\mathbf{F};\theta)$ to find all the different equilibrium paths and their stability of a stress-free bi-atomic perfect crystal as a function of temperature. In this work we investigate the influence of hydrostatic pressure. In general, hydrostatic compression increases the critical temperatures on the principal branches. For the same absolute value, hydrostatic tension is found to have a more pronounced effect on the equilibrium paths than hydrostatic compression.

Keywords: Stability; Symmetry phases; Crystal; Compression

1. Introduction

First-order displacive (martensitic) phase transformations between solid state phases are the underlying mechanism responsible for the technologically important thermo-mechanical properties of shape memory alloys (SMAs). These properties are the shape memory affect and the pseudo-elastic behavior. The first refers to the capacity of the alloy to erase relatively large (up to 8%) mechanically-induced strains by moderate temperature increases. The second pertains to the ability of the alloy to accommodate strains of this magnitude and recover upon unloading via a hysteretic stress–strain loop.

Of the long list of alloys that have these remarkable properties, NiTi-based alloys have the best memory properties as polycrystals, and as a result, are the most popular and commercially viable. It is for this

* Corresponding author. Fax: +1-734-763-0578.
E-mail address: jashaw@umich.edu (J.A. Shaw).

0020-7683/02/$ - see front matter
PII: S0020-7683(02)00183-X

reason that the present work is focused on an ordered equi-atomic binary alloy as our prototype for a shape memory alloy.

Instabilities at the nanoscale, via the transition from cubic (austenite) to monoclinic (detwinned martensite) phases, can manifest themselves at the polycrystalline macroscale through complicated mechanisms of localization and propagating transformation fronts. The modelling of discontinuous strain fields (e.g. Shaw and Kyriakides, 1998; Shaw, 2000) implies serious technical problems (due to the loss of ellipticity of the governing equations). This is one of a number of issues that perhaps explains why the continuum level thermomechanical description of SMAs has lagged behind their materials science understanding.

Thanks to the work of Abeyaratne, Bhattacharya, Ericksen, James, Knowles and many others, a continuum mechanics methodology based on finite strain thermoelasticity has taken shape since the early 1980s. This approach consists of assuming the existence of a phenomenological energy density $W(\mathbf{F},\theta)$ (where $\mathbf{F}$ is the deformation gradient and θ is the absolute temperature) with local minima in $\mathbf{F}$ (potential wells) that correspond to different stable phases of the crystal (see James, 1986). This approach has been satisfactory in predicting the fine microstructures observed in SMAs (e.g. see Abeyaratne et al. (1996) for application to laminar microstructures of CuAlNi). The same framework has also been adopted by Ericksen (1992), who uses symmetry properties of the perfect crystals to show different equilibrium paths can emerge as bifurcated solutions from the principal branch of the higher symmetry austenitic (cubic) phase.

However, important questions pertaining to which phases can coexist at a certain temperature remain unanswered by the phenomenological construction of W. One reasonable way to improve the situation is to derive the corresponding energy density from temperature dependent atomic potentials. For purely mechanical loadings and mono-atomic cubic crystals this approach to studying the stability of crystals can be traced back to Born (1940). More recently Milstein and Hill (1977, 1978, 1979) studied the dependence of bulk and shear moduli of such crystals and their dependence on hydrostatic pressure. In a recent paper, Elliott et al. (in press) introduced thermally-dependent atomic potentials to explicitly derive $W(\mathbf{F},\theta)$ and studied the resulting symmetry breaking stress-free bifurcated equilibrium paths and their stability.

The next logical step is to investigate the influence of stress on the temperature dependent equilibrium paths and their stability. As a first step, the present work studies the response of an infinite, perfect bi-atomic crystal under hydrostatic pressure. Following a brief description of the model in Section 2 we discuss the existence of critical points on principal equilibrium branches (cubic crystals) and the character of the emerging bifurcated branches (lower symmetry crystals) in Section 3. The results of the numerical calculations are discussed in Section 4.

2. Problem statement

The boundary value problem of interest consists of an infinite lattice with boundary conditions consistent with an external hydrostatic pressure p. The lattice is subjected to a uniform *symmetric* deformation $\mathbf{U} = \mathbf{U}^{\mathrm{T}}$ (there is no loss of generality in this assumption—it simply excludes rigid body rotations). Consequently the relative current position vector $\mathbf{r}_{ij} \equiv \mathbf{r}_j - \mathbf{r}_i$ is related to its reference counterpart $\mathbf{R}_{ij} \equiv \mathbf{R}_j - \mathbf{R}_i$ by

$$\mathbf{r}_{ij} = \mathbf{U} \cdot \mathbf{R}_{ij}, \tag{2.1}$$

where $(\cdot)$ indicates simple tensor contraction ($\mathbf{A} \cdot \mathbf{B} = A_{ij}B_j$). Assuming that ϕ_i, the atomic potential of atom i, is a function of the current position vectors $\mathbf{r}_{ij}$, where $j \neq i$ denotes all other lattice positions, the free energy density, W, of the crystal at temperature θ is

$$W(\mathbf{U};\theta) = \frac{1}{2V_{\mathrm{r}}} \sum_{i=1}^{K} \phi_i(\mathbf{r}_{i1}, \mathbf{r}_{i2}, \ldots, \mathbf{r}_{i(i-1)}, \mathbf{r}_{i(i+1)}, \ldots; \theta). \tag{2.2}$$

In the above expression V_r is the reference volume of the unit cell and K is the number of atoms in the unit cell. For the case of a crystal subjected to a hydrostatic pressure p, the corresponding total energy of the system per unit reference volume is

$$\mathscr{E}(\mathbf{U};\theta,p) = W(\mathbf{U};\theta) + p\det\mathbf{U}, \tag{2.3}$$

where p is assumed positive in compression. The conservative system's equilibrium solutions at a given temperature and pressure are found by extremizing its energy with respect to $\mathbf{U}$, namely

$$\frac{\partial\mathscr{E}}{\partial\mathbf{U}} = \frac{\partial W}{\partial\mathbf{U}} + p\det(\mathbf{U})\mathbf{U}^{-1} = \mathbf{0}. \tag{2.4}$$

A solution to the above equation is a stable equilibrium point if it is a local minimizer of $\mathscr{E}$ with respect to $\mathbf{U}$, i.e. if

$$\min\left[\delta\mathbf{U} : \frac{\partial^2\mathscr{E}}{\partial\mathbf{U}\partial\mathbf{U}} : \delta\mathbf{U}\right] > 0, \tag{2.5}$$

over all positive definite, symmetric rank two tensors $\delta\mathbf{U}$. Here (:) indicates double tensor contraction ($\mathbf{A} : \mathbf{B} = A_{ijkl}B_{kl}$).

Although the energy density W can be calculated for any type of atomic potential, a pair potential will be used in the following calculations for reasons of computational simplicity. For the case of an ordered bi-atomic CsCl-type crystal (the austenite phase of NiTi) with atom species a and b, the internal energy density of the crystal simplifies to

$$W(\mathbf{U};\theta) = \frac{1}{2V_r}\left\{\sum_i\left[\phi_{aa}(r_{ai};\theta) + \phi_{ab}(r_{bi};\theta)\right] + \sum_j\left[\phi_{bb}(r_{bj};\theta) + \phi_{ab}(r_{aj};\theta)\right]\right\}, \tag{2.6}$$

where the subscripts a and b on r denote the corresponding atoms in a unit cell, i and j range over all a and b atoms respectively within a sphere of influence, and ϕ_{aa}, ϕ_{ab}, ϕ_{bb} denote the pair potentials between atom-types a–a, a–b, and b–b, respectively.

The temperature-dependent Morse-type pair potential $\phi(r;\theta)$ adopted for the ensuing numerical calculations has been introduced by Elliott et al. (in press), namely

$$\phi(r;\theta) = A(\theta)\left\{\exp\left[-2m(\theta)\left(\frac{r}{\hat{r}(\theta)} - 1\right)\right] - 2\exp\left[-m(\theta)\left(\frac{r}{\hat{r}(\theta)} - 1\right)\right]\right\}, \tag{2.7}$$

where the bond strength $A(\theta)$, bond stiffness parameter $m(\theta)$ and bond length $\hat{r}(\theta)$ are given by

$$\begin{aligned} A(\theta) &= A_0\left[1 - \frac{\theta}{4\theta_m}\right], \\ m(\theta) &= m_0\left[1 + \alpha_\theta\frac{(\theta - \theta_r)}{\theta_r}\right], \\ \hat{r}(\theta) &= r_0\left[1 - \frac{1}{2m_0}\ln\left(1 - \frac{\theta}{4\theta_m}\right)\right]. \end{aligned} \tag{2.8}$$

Here θ_r is the reference temperature, r_0 is the bond length at $\theta = 0$, θ_m is the melting temperature, A_0 is the binding energy, m_0 is the bond stiffness parameter, and α_θ is the stiffness temperature coefficient. It is understood that the above defined pair potentials and their coefficients depend on the bond type a–a, a–b, or b–b, but these indices are omitted in (2.7), (2.8) in the interest of notational simplicity.

Based on the above presented equations, we seek the solutions of (2.4) (as a function of the temperature for a particular pressure) and investigate their stability.

3. Critical points and stability of principal branches

Despite its apparent simplicity, the tensor Eq. (2.4) consists of six nonlinear equations. Due to the cubic symmetry of the reference configuration, the simplest and most obvious solution is a uniform dilation $\overset{0}{\mathbf{U}}(\theta,p)=\lambda(\theta,p)\mathbf{I}$ ($\mathbf{I}$ the rank two identity tensor) which is termed the "*principal solution*" and which corresponds to the austenite phase with a CsCl crystal structure. For relatively low pressures, it is reasonable to assume that the austenite (principal) phase $\overset{0}{\mathbf{U}}$ is stable, i.e. that the corresponding minimum eigenvalue of $\partial^2\mathscr{E}/\partial\mathbf{U}\partial\mathbf{U}$ is positive, at least near the reference temperature θ_r, defined as the temperature where $\lambda(\theta_r,0)=1$. When the temperature decreases away from θ_r, it reaches a value $\theta_c(p)$, termed the "*critical temperature*" at which the austenite phase $\overset{0}{\mathbf{U}}$ looses positive definiteness of $\mathscr{E}$, i.e.

$$\frac{\partial^2\mathscr{E}\left(\overset{0}{\mathbf{U}}(\theta_c(p),p);\theta_c(p),p\right)}{\partial\mathbf{U}\partial\mathbf{U}}:\overset{(I)}{\mathbf{U}}=\mathbf{0};\quad (I=1,2,\ldots,N). \tag{3.1}$$

Here the N distinct eigenmodes $\overset{(I)}{\mathbf{U}}$ guide the search for lower symmetry equilibrium solutions which emerge from the principal branch at θ_c. The asymptotic construction of these post-bifurcated equilibrium paths uses the same methodology as the zero pressure case, which is presented in detail by Elliott et al. (in press), and hence needs not be repeated here. Only the classification of the critical points and their pressure dependence are discussed.

To this end, and due to the cubic symmetry of the crystal, (3.1) can be rewritten in component form as

$$\begin{bmatrix} L_{11}^c & L_{12}^c+p\lambda & L_{12}^c+p\lambda & 0 & 0 & 0\\ L_{12}^c+p\lambda & L_{11}^c & L_{12}^c+p\lambda & 0 & 0 & 0\\ L_{12}^c+p\lambda & L_{12}^c+p\lambda & L_{11}^c & 0 & 0 & 0\\ 0 & 0 & 0 & L_{44}^c-p^{\lambda/2} & 0 & 0\\ 0 & 0 & 0 & 0 & L_{44}^c-p^{\lambda/2} & 0\\ 0 & 0 & 0 & 0 & 0 & L_{44}^c-p^{\lambda/2} \end{bmatrix} \begin{bmatrix} U_{11}\\ U_{22}\\ U_{33}\\ 2U_{12}\\ 2U_{23}\\ 2U_{31} \end{bmatrix}^{(I)} = \mathbf{0}, \tag{3.2}$$

where

$$L_{11}^c\equiv\left.\frac{\partial^2 W}{\partial U_{11}^2}\right|_{\left(\overset{0}{\mathbf{U}}(\theta_c,p),\theta_c\right)},\quad L_{12}^c\equiv\left.\frac{\partial^2 W}{\partial U_{11}\partial U_{22}}\right|_{\left(\overset{0}{\mathbf{U}}(\theta_c,p),\theta_c\right)},\quad L_{44}^c\equiv\left.\frac{\partial^2 W}{\partial U_{12}^2}\right|_{\left(\overset{0}{\mathbf{U}}(\theta_c,p),\theta_c\right)}, \tag{3.3}$$

are the moduli of the cubic phase at the critical temperature.

The critical points on the principal solution path are thus found to be the zeros of the determinant of the 6×6 matrix in (3.2), namely

$$\left(L_{11}^c+2L_{12}^c+2p\lambda\right)\left(L_{11}^c-L_{12}^c-p\lambda\right)^2\left(L_{44}^c-p\lambda/2\right)^3=0. \tag{3.4}$$

These critical points are either limit loads or bifurcation points according to whether $\partial^2\mathscr{E}/\partial\mathbf{U}\partial\theta|_c:\overset{(I)}{\mathbf{U}}\neq 0$, or $=0$, respectively (see Triantafyllidis and Peek, 1992). Hence, for the case of the simple root of (3.4) ($N=1$, $L_{11}^c+2L_{12}^c+2p\lambda=0$) the corresponding unique eigenmode is $\overset{(1)}{\mathbf{U}}=\mathbf{I}$ and the above mentioned criterion shows that this critical point is a limit load.

For the case of the double root of (3.4) ($N=2, L_{11}^c-L_{12}^c-p\lambda=0$) a double bifurcation point exists with two independent eigenmodes:

$$\overset{(1)}{\mathbf{U}}=\begin{bmatrix}2&0&0\\0&-1&0\\0&0&-1\end{bmatrix},\quad \overset{(2)}{\mathbf{U}}=\begin{bmatrix}-1&0&0\\0&2&0\\0&0&-1\end{bmatrix}. \tag{3.5}$$

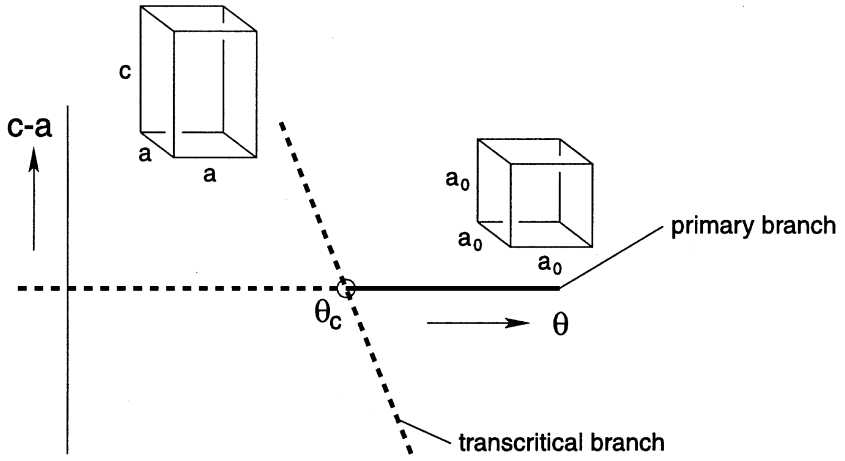

Fig. 1. Cubic to tetragonal bifurcation.

For this case, the asymptotic analysis presented in Elliott et al. (in press) shows that three different tetragonal phase branches (unit cell angles $\alpha = \beta = \gamma = \pi/2$, sides $a = b \neq c$) emerge at θ_c from the principal cubic phase in an asymmetric, transcritical type bifurcation depicted schematically in Fig. 1. It can also be shown that all three tetragonal branches are unstable in the neighborhood of θ_c, independent of the interatomic potential.

Finally, for the case of the triple root of (3.4) ($N = 3$, $L^c_{44} - p\lambda/2 = 0$), a triple bifurcation point exists with three independent eigenmodes:

$$\overset{(1)}{\mathbf{U}} = \begin{bmatrix} 0 & 0 & 0 \\ 0 & 0 & 1 \\ 0 & 1 & 0 \end{bmatrix}, \quad \overset{(2)}{\mathbf{U}} = \begin{bmatrix} 0 & 0 & 1 \\ 0 & 0 & 0 \\ 1 & 0 & 0 \end{bmatrix}, \quad \overset{(3)}{\mathbf{U}} = \begin{bmatrix} 0 & 1 & 0 \\ 1 & 0 & 0 \\ 0 & 0 & 0 \end{bmatrix}. \tag{3.6}$$

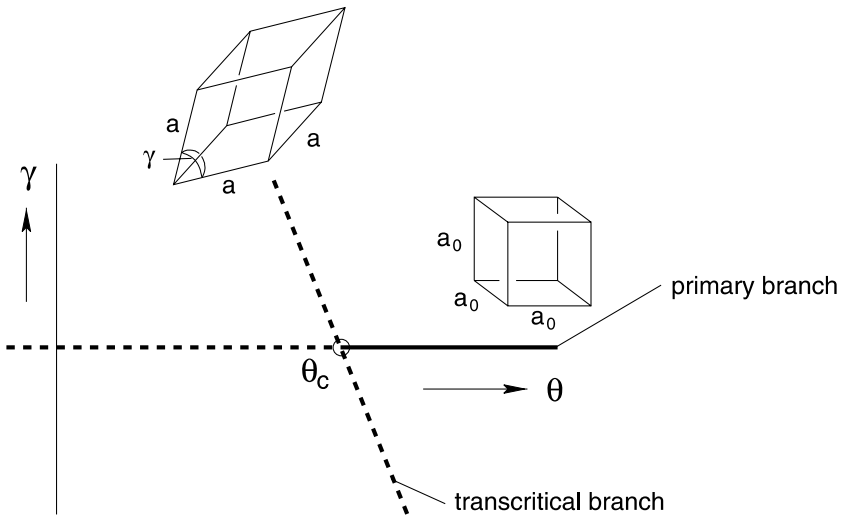

Fig. 2. Cubic to rhombohedral bifurcation.

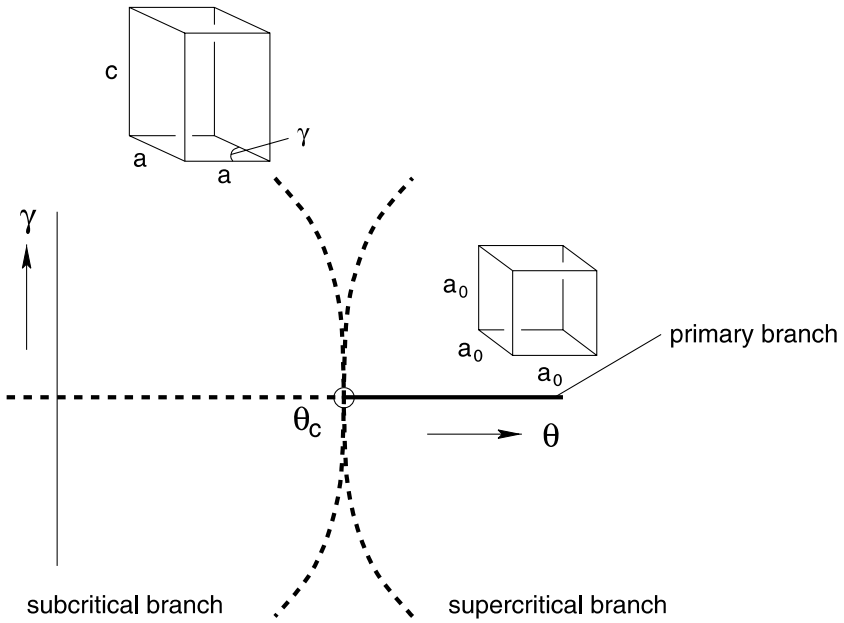

Fig. 3. Cubic to orthorhombic bifurcation.

For this case, the asymptotic analysis shows that seven different equilibrium paths emerge at θ_c. Four of these paths correspond to different variants of a rhombohedral phase (unit cell angles $\alpha = \beta = \gamma \neq \pi/2$, sides $a = b = c$) which result by stretching the cubic unit cell along each one of its four main diagonals. Each one of these paths is an asymmetric, transcritical type bifurcation depicted schematically in Fig. 2 which can be shown to be unstable in the neighborhood of θ_c, independent of the choice of the interatomic potential. The remaining three equilibrium paths emerging from θ_c correspond to different variants of an orthorhombic phase (unit cell angles $\alpha = \beta = \pi/2, \gamma \neq \pi/2$, sides $a = b \neq c$) which result by shearing two opposite faces of the cube and allowing the perpendicular edge to stretch independently. The corresponding bifurcations are symmetric and are depicted schematically in Fig. 3. In the neighborhood of θ_c they can be stable or unstable, and supercritical or subcritical, depending on the choice of the interatomic potential.

4. Numerical results

Having gained a clear understanding of the character of the bifurcated equilibrium paths near the critical points, we turn our attention to numerical calculations of the entire equilibrium paths in a temperature

Table 1
Pair potential parameters used in numerical calculation

Parameter	*a–a* bond	*b–b* bond	*a–b* bond
r_0	1	1.16	1.08
θ_m	1718	1943	1573
A_0	1	1.124	0.425
m_0	4	7	5.5
α_θ	0	0	3

range of 100 K (220 K $\leqslant \theta \leqslant$ 320 K) and for angles γ in the range $30° \leqslant \gamma \leqslant 120°$. The parameters chosen for the three different types of pair potentials are given in Table 1. The parameters of the like bonds are chosen to give reasonable moduli (ratios) and thermal expansion coefficients near room temperature, which is also chosen as the reference temperature ($\theta_r = 300$ K). The parameters of the unlike bond are chosen so that the crystal is stable in the CsCl crystal structure for $\theta \geqslant \theta_r$. The bifurcated equilibrium paths are calculated as functions of temperature for three different fixed values of the dimensionless pressure $P = 0.1$ (compression), 0, and -0.1 (tension) with $P \equiv p/G$ where $G \equiv L_{44}^{c}(\overset{0}{\mathbf{U}}(\theta_r, 0), \theta_r)$ the shear modulus at the reference temperature and zero pressure.

The numerical solution of (2.4) is accomplished through an incremental Newton–Raphson method which is described in Elliott et al. (in press). There are four types of equilibrium paths found in our numerical calculations (each corresponding to a different lattice symmetry) which are listed below according to the increasing number of the degrees of freedom required for their description

$$\mathbf{U}_{\text{cubic}} = \begin{bmatrix} U_{11} & 0 & 0 \\ 0 & U_{11} & 0 \\ 0 & 0 & U_{11} \end{bmatrix}, \tag{4.1a}$$

$$\mathbf{U}_{\text{rhombo}} = \begin{bmatrix} U_{11} & U_{12} & U_{12} \\ U_{12} & U_{11} & U_{12} \\ U_{12} & U_{12} & U_{11} \end{bmatrix}, \tag{4.1b}$$

$$\mathbf{U}_{\text{ortho}} = \begin{bmatrix} U_{11} & U_{12} & 0 \\ U_{12} & U_{11} & 0 \\ 0 & 0 & U_{33} \end{bmatrix}, \tag{4.1c}$$

$$\mathbf{U}_{\text{mono}} = \begin{bmatrix} U_{11} & U_{12} & U_{13} \\ U_{12} & U_{11} & U_{13} \\ U_{13} & U_{13} & U_{33} \end{bmatrix}. \tag{4.1d}$$

An arc length continuation method avoids numerical difficulties associated with limit loads. The stability of each equilibrium point on every path is evaluated by finding the eigenvalues of $\partial^2 \mathscr{E}/\partial \mathbf{U} \partial \mathbf{U}$ using a cyclic Jacobi method (see Patel, 1994). The same method identifies zero eigenvalues which signal the presence of bifurcation points on an equilibrium path and hence the need to search for emerging branches with lower (or possibly higher) symmetry (assuming of course that the critical point is not a limit load).

The results of the numerical calculations are shown in Figs. 4–6. In Fig. 4 constant pressure graphs are plotted for the lattice angle $\gamma(\cos(\gamma) = U_{1k}U_{2k})$ versus temperature. The baseline case (already presented in Elliott et al. (in press)) is Fig. 4(b) which corresponds to the pressure-free crystal, while Fig. 4(a) and (c) correspond to hydrostatic compression ($P = 0.1$) and tension ($P = -0.1$), respectively. There are certain common features shared by the three graphs. The CsCl cubic crystal ($\gamma = 90°$) is stable (solid line) for the higher temperature range and unstable (dotted line) for the lower temperature range of the graph. A triple bifurcation point occurs at about $\theta_c(P = 0) = 263$ K and four rhombohedral and three orthorhombic paths emerge from this critical point as discussed in the previous section, but only one representative path from each is shown here. We observe that the rhombohedral path is initially unstable and asymmetric about the principal branch and that the orthorhombic path is symmetric, respectively, as expected from the asymptotic analysis. For our particular choice of atomic potential, the orthorhombic path is unstable also.

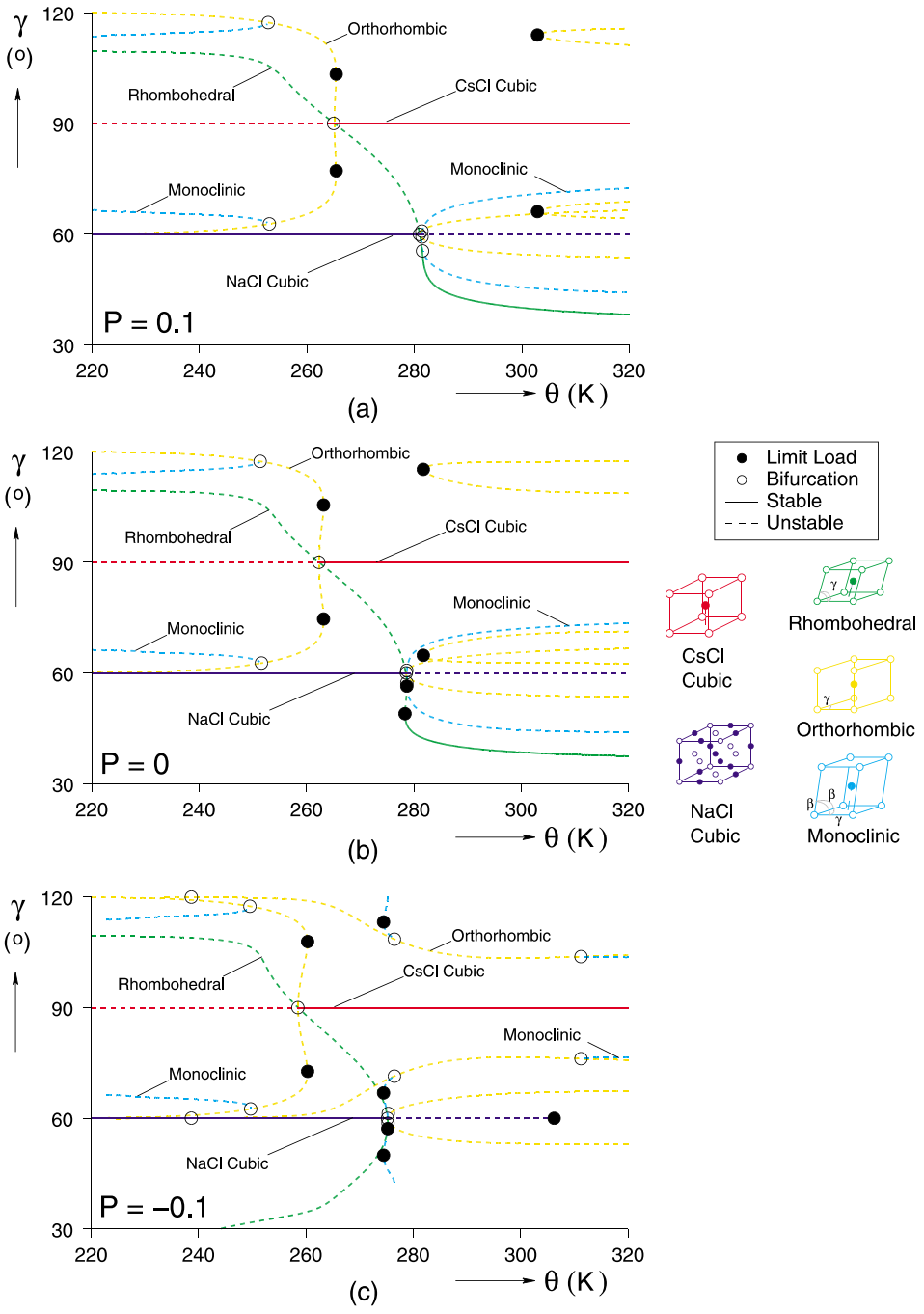

Fig. 4. Calculated equilibrium paths showing unit cell angle as a function of temperature for three different pressures.

Another common feature of the three cases is the presence of a branch with a cubic NaCl structure at $\gamma = 60°$. The presence of this equilibrium branch, which corresponds to a reconstructive transformation

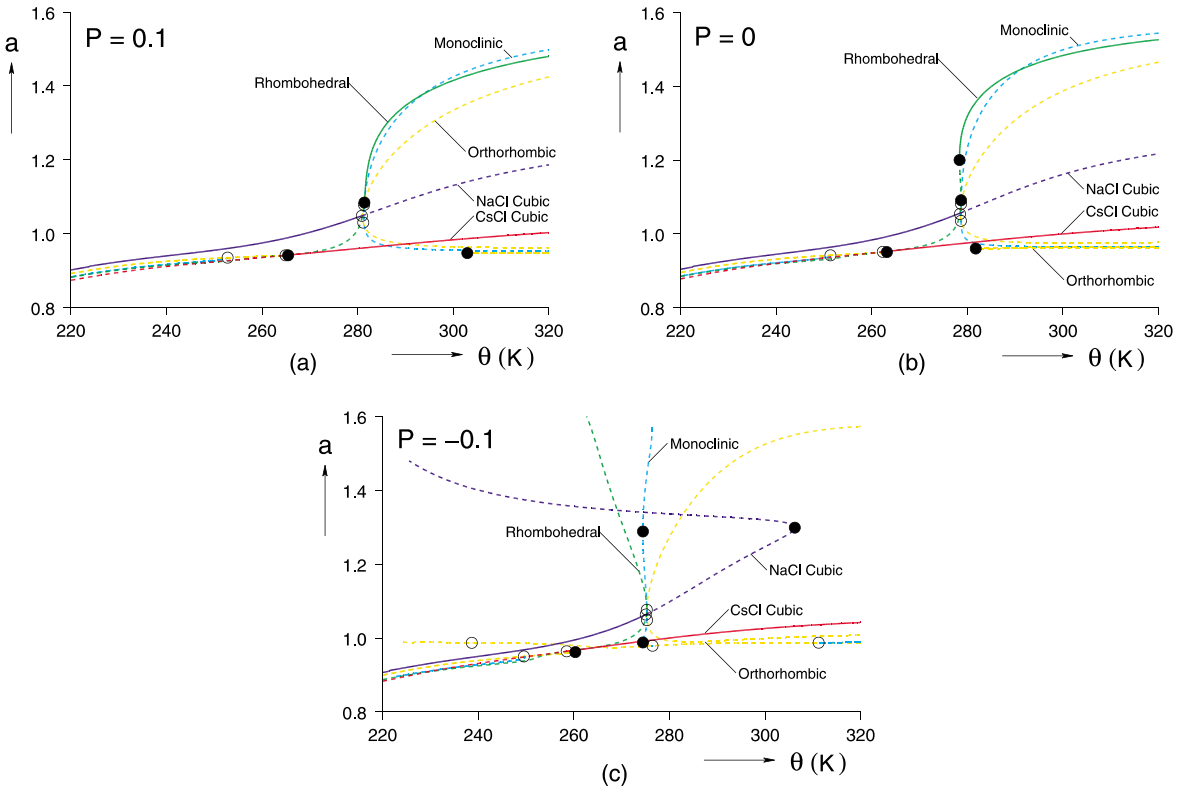

Fig. 5. Unit cell side-length as a function of temperature for three different pressures.

from the CsCl configuration, has been discussed in Elliott et al. (in press). A triple bifurcation point is also found on the NaCl branch, but at a higher temperature than that of the CsCl branch. In addition, the NaCl path's stability is reversed as compared to the CsCl path, i.e. it is unstable for the higher range of temperatures and stable for the lower range of temperatures in the graph. In fact, a similar structure change actually occurs in the CsCl ionic compound near 460 °C above which it transforms to a NaCl-like structure (see Buerger (1951), which refers to this as a dilatational transformation). The observations about the nature of the bifurcation paths through the critical point on the NaCl branch, i.e. the symmetry/asymmetry of the paths and their stability, carry over from the discussion of the triple bifurcation point on the CsCl branch and need not be repeated.

Looking now at the influence of hydrostatic compression on the equilibrium paths, we see no qualitative difference between Fig. 4(a) and (b), except for the absence of the two limit loads in the rhombohedral path near the NaCl triple bifurcation point in Fig. 4(a). The slight increase (of the order of 2 K) of the critical temperature at the triple bifurcation point on the CsCl branch in Fig. 4(a) as compared to Fig. 4(b) can be explained by studying the triple root in (3.4). At criticality the shear modulus for the CsCl branch is $L_{44}^{c} = p\lambda/2$. Since L_{44} depends on the pressure through the slowly changing normal strain of the branch $\lambda(\theta, p)$ (see red line in Fig. 5(a)) $L_{44}^{c} > 0$ at criticality (since $p\lambda/2 > 0$), the critical point shifts towards a higher temperature. According to this argument, the opposite should have been true for the shifting of the critical point on the NaCl branch (i.e. θ_c should be lower than in the stress free case), however in this case $\lambda(\theta, p)$ is more sensitive to pressure (see blue lines in Fig. 5) and results in a positive shifting of θ_c as well.

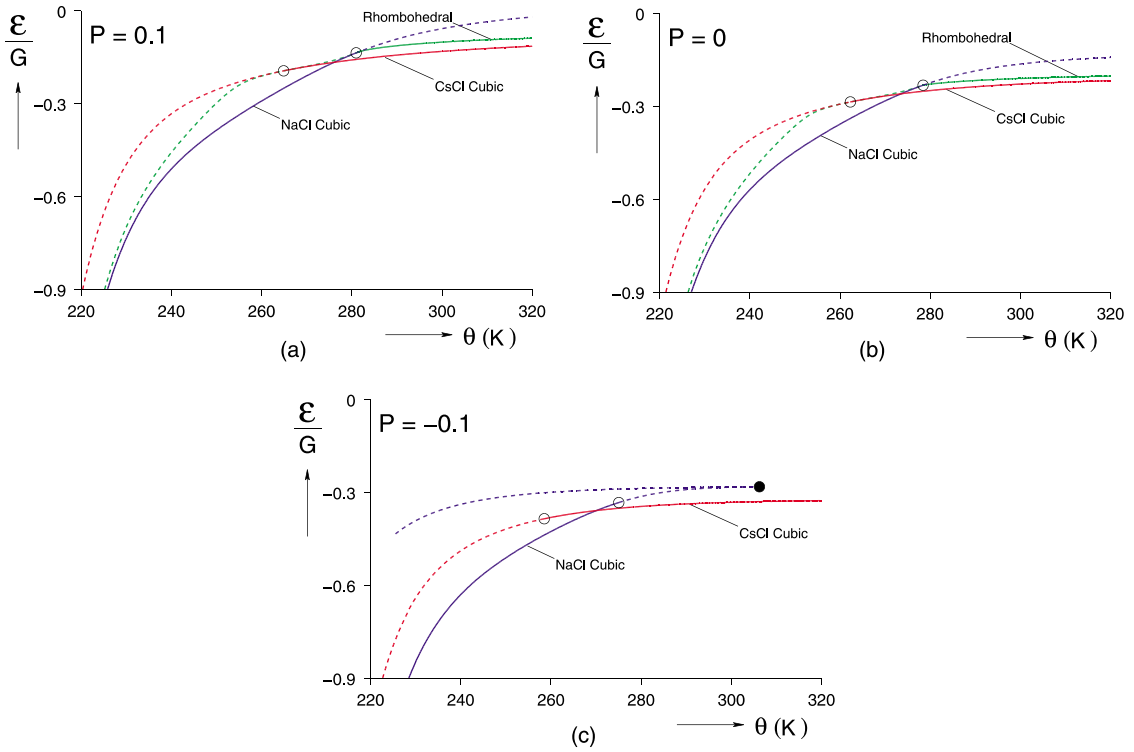

Fig. 6. Dimensionless energy density of stable equilibrium paths as a function of temperature for three different pressures.

The influence of the hydrostatic tension on the equilibrium paths of the crystal is more pronounced than that of hydrostatic compression (for the same, relatively large, absolute value of the dimensionless pressure) as revealed by comparing Fig. 4(b) and (c). Consistent with the above discussion, the critical points on the two cubic branches occur at lower temperatures than their stress-free counterparts. Notice the absence of the rhombohedral branch above a temperature of about 278 K for hydrostatic tension in Fig. 4(c). Moreover, the entire rhombohedral branch is unstable. Another important difference is that the NaCl cubic branch reaches a limit point at about 306 K.

The results of the same numerical calculations that were depicted in Fig. 4 are plotted in Fig. 5 in the form of unit cell side length a ($a = (U_{1k}U_{1k})^{1/2}$) versus temperature. As expected from the discussion of Fig. 4, hydrostatic compression has a relatively minor influence on a, as evidenced by comparing the graphs in Fig. 5(a) and (b). There is, however, a significant influence of hydrostatic tension, as observed in particular by the evolution of the side of the cubic NaCl path in Fig. 5(c). In contrast to the zero or compressive pressure cases, for tension two NaCl equilibrium configurations are found with substantially different unit cell sizes for temperatures below about 306 K, while no NaCl branch exists above this temperature.

Finally, the dimensionless energy $\mathscr{E}/G$ of the stable equilibrium paths is depicted in Fig. 6 for the same values of the dimensionless pressure. Notice that for lower temperatures in these graphs the NaCl branch is stable and has the lowest energy, while for the higher temperatures the CsCl branch is the stable, lowest energy branch. The stable rhombohedral branch, whenever it exists always has higher energy than the CsCl branch. As discussed in Elliott et al. (in press) the overlap of stable branches of the two cubic structures is suggestive of a hysteretic, temperature-induced, reconstructive transformation. Hydrostatic compression has the effect of shifting this overlap regime towards somewhat higher temperatures.

5. Summary and conclusions

The temperature-dependent atomic pair potential model for uniformly strained perfect bi-atomic crystals of infinite extent, which was introduced by Elliott et al. (in press) is extended to include the effects of hydrostatic pressure. Using temperature as the loading parameter, equilibrium paths are calculated and compared for three different values of the hydrostatic pressure $p = 0.1G$, $p = 0$, and $p = -0.1G$ (where G is the shear modulus of the lattice at the reference temperature and zero pressure). Within a certain range of temperature and unit cell angle we have identified all the equilibrium branches which are continuously connected with the principal path of a cubic, CsCl crystal structure.

The main conclusion of our study is that hydrostatic compression causes a shift of the critical points on the principal paths towards higher temperatures. In addition, compression produces smaller changes to the equilibrium solutions of the system than a hydrostatic tension of the same magnitude. In this case only two stable branches remain, each corresponding to a crystal with cubic symmetry.

The efforts made here are a first attempt to include the influence of applied mechanical stress on the nano-mechanical model of Elliott et al. (in press). The model presented here lacks the existence of a stable low symmetry equilibrium solution path. Such a path is an important feature of any material which exhibits the shape memory effect (see Bhattacharya, 1998). The authors believe that the addition of new kinematical degrees of freedom (such as the "shuffles" observed in the NiTi $B2 \rightarrow B19'$ transformation) or better atomic potentials such as the modified embedded atom method (MEAM, see Baskes, 1987) potentials (which can capture the angular bonding characteristics of many metals) are likely to help rectify this deficiency. Although further improvements are necessary for a more realistic modeling of SMAs, the proposed nano-mechanical framework has shown its usefulness as a fundamental vehicle for further studies.

Acknowledgements

The financial support from a Computational Science Graduate Fellowship from the Department of Energy (for R. Elliott) and a CAREER grant from the National Science Foundation (for J. Shaw) are acknowledged with thanks.

References

Abeyaratne, R., Chu, C., James, R.D., 1996. Kinetics of materials with wiggly energies: Theory and application to the evolution of twinning microstructures in a Cu–Al–Ni shape memory alloy. Philosophical Magazine A-Physics of Condensed Matter defects and Mechanical Properties 73 (2), 457–497.

Baskes, M.I., 1987. Application of the embedded-atom method to covalent materials: a semiempirical potential for silicon. Physical Review Letters 59 (23), 2666–2669.

Bhattacharya, K., 1998. Theory of martensitic microstructure and the shape-memory effect. Available from: <bhatta@co.caltech.edu>.

Born, M., 1940. On the stability of crystal lattices I. Mathematical Proceedings of the Cambridge Philosophical Society 36, 160–172.

Buerger, M.J., 1951. Crystallographic aspects of phase transformations. In: Smoluchowski, R. (Ed.), Phase Transformations in Solids. John Wiley, New York, pp. 183–211.

Elliott, R.S., Shaw, J.A., Triantafyllidis, N., 2002. Stability of thermally-induced martensitic transformations in bi-atomic crystals. Journal of the Mechanics and Physics of Solids, in press.

Ericksen, J.L., 1992. Bifurcation and martensitic transformations in Bravais lattices. Journal of Elasticity 28, 55–78.

James, R.D., 1986. Displacive phase transformations in solids. Journal of the Mechanics and Physics of Solids 34 (4), 359–394.

Milstein, F., Hill, R., 1977. Theoretical properties of cubic crystals at arbitrary pressure—I. Density and bulk modulus. Journal of the Mechanics and Physics of Solids 25, 457–477.

Milstein, F., Hill, R., 1978. Theoretical properties of cubic crystals at arbitrary pressure—II. Shear moduli. Journal of the Mechanics and Physics of Solids 26 (4), 213–239.

Milstein, F., Hill, R., 1979. Theoretical properties of cubic crystals at arbitrary pressure—III. Stability. Journal of the Mechanics and Physics of Solids 27 (3), 255–279.

Patel, V.A., 1994. In: Numerical Analysis. Saunders College Publishing, Fort Worth, TX, pp. 440–445 (Chapter 13).

Shaw, J.A., Kyriakides, S., 1998. Initiation and propagation of localized deformation in elasto-plastic strips under uniaxial tension. International Journal of Plasticity 13 (10), 837–871.

Shaw, J.A., 2000. Simulations of localized thermo-mechanical behavior in a NiTi shape memory alloy. International Journal of Plasticity 16 (5), 541–562.

Triantafyllidis, N., Peek, R., 1992. On stability and the worst imperfection shape in solids with nearly simultaneous eigenmodes. International Journal of Solids and Structures 29 (18), 2281–2299.